Ocean Engineering 113 (2016) 151–161

Contents lists available at ScienceDirect

Ocean Engineering

journal homepage: www.elsevier.com/locate/oceaneng

Vector field path following for surface marine vessel and parameter identification based on LS-SVM

Haitong Xu, C. Guedes Soares *

Centre of Marine Technology and Ocean Engineering (CENTEC), Instituto Superior Técnico, Universidade de Lisboa, Av. Rovisco Pais, 1049-001 Lisboa, Portugal

ARTICLE INFO

Article history:
Received 6 July 2015
Accepted 17 December 2015
Available online 13 January 2016

Keywords:
Autonomous surface vehicle
Path following control
Parameter identification
Vector field
Line of sight

ABSTRACT

A two-dimensional path following control system for autonomous surface vehicles is presented. The guidance system is obtained through a way-point guidance scheme based on a vector field algorithm. Vector field is a simple and robust method and its stability is proved using Lyapunov stability criteria. The 2-degree of freedom (sway-yaw) linear manoeuvring model is chosen as the control model and the parameters are obtained by using the least-square support vector regression. The sensitivity of the vector field algorithm to its parameters is studied and simulation tests are presented to compare the performance of the tradition line-of-sight scheme and vector field algorithm. The results show that the vector field has a better performance for autonomous surface vehicle's path following control, is a practical and robust method for accurate path following, and can be extended to higher dimensional control and guidance problems.

1. Introduction

Autonomous surface vehicles have demonstrated their usefulness in last decades. They can be used for various missions in civil and commercial fields, such as marine survey, coastal and inland monitoring, etc. Guidance systems are critical important for the overall performance of autonomous surface vehicles, because they are concerned with the transient motion behaviour associated with the achievement of motion control objectives (Breivik and Fossen, 2009). Path following is one of the typical control scenarios in the control literature and it pertains to following a predefined path (Lekkas and Fossen, 2014). The predefined path is usually specified in terms of way-points (Fossen, 2002), and is selected considering some features like weather conditions (Vettor and Guedes Soares, 2015), sea states (Chen et al., 2013), obstacles avoidance, missions, economic and control effort. Way-points are defined in Cartesian coordinates in the inertial reference frame (Fossen, 2011). The path between the waypoints is usually generated using a straight line or other algorithms such as monotone CHSI algorithm (Lekkas and Fossen, 2014). In this paper we consider the problems of designing a controller that makes the ship follow the straight lines between way-points, and controls the forwards speed to a possibly time-varying desired speed.

The basic requirement of path-following algorithm is that they must be accurate and robust to environment disturbances (Sujit et al., 2014). In recent years, path-following based on the Line-of-Sight (LOS) is widely used for autonomous surface vehicles. The LOS guidance algorithm and its properties have been studied thoroughly in the literatures. An overview of the LOS path-following algorithms for marine vehicles is presented by Lekkas and Fossen (2013), which also discussed the form of the path and path evaluation criteria. In Fossen (2011), a nonlinear mathematical model for ship manoeuvring and LOS path-following is studied. The scale model tests are carried out and the results indicate that the LOS path-following controller is capable of tracking the path. In order to improve the speed of the convergence of the vehicle to the desired path, Moreira et al. (2007) present a new approach concerning the calculation of a dynamic Line-of-Sight vector norm. Further study can be found in (Moreira and Guedes Soares, 2011; Sutulo et al., 2002). Loe (2008) presented a modified version of the LOS algorithm, which is a bit gentler and never tries to steer the ship directly towards the path.

In order to prove the stability of the LOS algorithm, Børhaug and Pettersen (2005) presented a cascaded systems approach. In that paper, the LOS guidance system achieves globally κ-exponential stabilisation using the sliding mode controller. In Fredriksen and Pettersen (2006), a LOS control law, which can globally κ-exponential stabilise an underactuated ship in 3-DOF, is derived using cascaded control theory. The theory is verified by the model tests. A uniform semi global exponential stability

* Corresponding author. Tel.: +351 218417957.
E-mail address: c.guedes.soares@centec.tecnico.ulisboa.pt (C. Guedes Soares).

http://dx.doi.org/10.1016/j.oceaneng.2015.12.037
0029-8018/

(USGES) proof for a class of proportional line-of-sight guidance laws used for vehicle path-following control is presented in Fossen and Pettersen (2014). The USGES stability property is important for systems that are exposed to environmental disturbances.

The vector field approach is a well-known tool for guidance problems in the area of UAV (Lim et al., 2014). Nelson et al. (2006, 2007) presented the vector field method for unmanned aerial vehicles path following. The experiment was carried out and the results validate the effectiveness of the vector field approach. Frew et al. (2008) proved the stability of the vector filed by using Lyapunov stability theory. Gonçalves et al. (2010) presents a time-varying vector field based approach. The vector field can be applied to not only path following, but also other purposes such as arrival position, angle, and time control (Lim et al., 2014). Although the vector field technique is widely using in the path following of UAV, there are a few literature about the vector field path-following guidance technique in the Autonomous Surface Vehicles. Owing to its many advantages, it is necessary to carry out research on the performance of the guidance system of ASVs using vector field technique.

The main contribution of this paper is the design the ASV's control system based on a waypoint guidance algorithm using vector field, which is used to compute the desired heading angle. The stability of the vector field is analysed using Lyapunov function. In addition, a tracking controller including a feedforward term and speed controller obtained through state feedback linearization are developed. A PID heading controller is derived and its gains are obtained from a 2-DOF (sway-yaw) linear manoeuvring model. The parameters are identified using Least Square Support Vector Machine, which is widely used in identification of ship hydrodynamic coefficients (Luo et al., 2013; Luo and Zou, 2009; Zhang and Zou, 2011; Moreno-Salinas et al., 2013). Simulation test based on the mathematical model of the ASV is carried out to analysis the sensitivity of the vector field algorithm to its parameters. Another simulation tests are also presented to compare the performance of the LOS and vector field algorithms. The results show that ASV have a better performance using vector field, which is a practical and robust method for accurate path following, and can be extended to higher dimensional control and guidance problems.

2. Mathematical model of "Esso Osaka"

In this section, the zigzag simulation is carried out using the "Esso Osaka" ship model (Fig. 1), the manoeuvring performance of "Esso Osaka" ship model has been studied thoroughly and there is rich experimental data. An "Esso Osaka" model was constructed and model tests were carried out as described in (Moreira and Guedes Soares, 2011) and one guidance, control and navigation platform has been developed by Perera et al. (2012) so that the

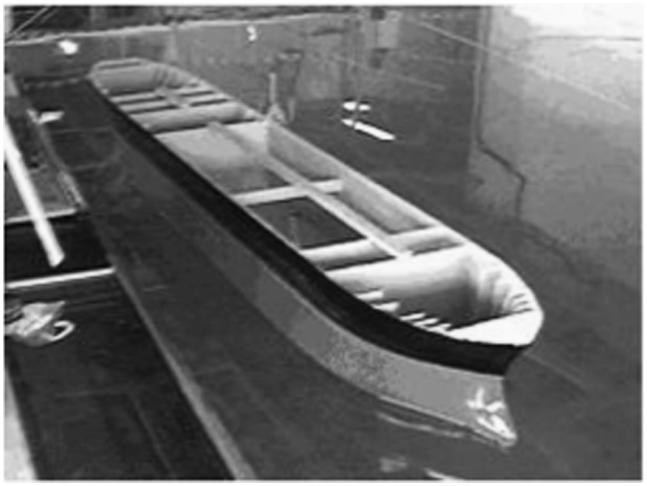

Fig. 1. The "Esso Osaka" ship model (adapted from Moreira et al., 2007).

ASV can perform a set of manoeuvring tests autonomously. The model was scaled 1:100 from the real ship. The main characteristics are listed in Table 1 and the nondimensional hydrodynamic coefficients, which are used to simulate the "Esso Osaka" trial manoeuvres, are presented in Table 2.

The simulation equation used in this paper is the one presented in Abkowitz (1980). Considering the environment disturbances, such as wind current and waves, and the small above water structure of the "Esso Osaka" ship model, the current effect is considered as the main external excitation. If u_c is the current's magnitude, α is the current's direction, ψ is the ship's heading angle, u is the forward component of velocity over ground, and v is the transverse component of velocity, the relative forward velocity u_r and transverse velocity v_r are given by

$$\begin{cases} u_r = u - u_c \cos(\psi - \alpha) \\ v_r = v + u_c \sin(\psi - \alpha) \end{cases} \tag{1}$$

The resulting advance speed of the vehicle is given by

$$U_r = \sqrt[2]{u_r^2 + v_r^2} \tag{2}$$

The derivative with respect to time of u and are given by (Moreira et al., 2007)

$$\begin{cases} \dot{u} = \dot{u}_r - u_c r \sin(\psi - \alpha) \\ \dot{v} = \dot{v}_r - u_c r \cos(\psi - \alpha) \\ \dot{u}_r = \frac{f_1}{m - X_{\dot{u}_r}} \\ \dot{v}_r = \frac{1}{f_4}\left[(I_Z - N_{\dot{r}})f_2 - (mx_G - Y_{\dot{r}})f_3\right] \\ \dot{r} = \frac{1}{f_4}\left[(m - Y_{\dot{v}_r})f_3 - (mx_G - N_{\dot{v}_r})f_2\right] \end{cases} \tag{3}$$

where

$$\begin{cases} f_1 = \left[\frac{\rho}{2}L^2\right]\eta_1' u_r^2 + \left[\frac{\rho}{2}L^3\right]\eta_2' n u_r + \left[\frac{\rho}{2}L^4\right]\eta_3' n^2 - \left[\frac{\rho}{2}Su_r^2\right]C_R' + \left[\frac{\rho}{2}L^2\right]X_{vr}'' v_r^2 + \left[\frac{\rho}{2}L^2 c^2\right]X_{ee}' e^2 \\ \quad + \left[\frac{\rho}{2}L^4\right](X_{rr}' + m' x_G')r^2 + \left[\frac{\rho}{2}L^3\right]\left(X_{v_r r}' + m'\right)v_r r + \left[\frac{\rho}{2}L^4 U^{-2}\right]X_{v_r v_r rr}' v_r^2 r^2 \\ f_2 = \left[\frac{\rho}{2}L^2\left(\frac{u_{A\infty}}{2}\right)^2\right]Y_0' + \left\{\left[\frac{\rho}{2}L^2 U_r\right]Y_{vr}' v_r + \left[\frac{\rho}{2}L^2\right]Y_\delta'(c - c_0)v_r\right\} + \left\{\left[\frac{\rho}{2}L^3 U_r\right](Y_r' - m' u_r')r - \left[\frac{\rho}{2}L^3\right]\frac{Y_\delta'}{2}(c - c_0)r\right\} + \left[\frac{\rho}{2}L^2 c^2\right]Y_\delta'\delta + \left[\frac{\rho}{2}L^4 U_r^{-1}\right]Y_{v_r rr}' r^2 v_r + [\tfrac{\rho}{2}L^2 c^2]Y_{eee}' e^3 \\ f_3 = \left[\frac{\rho}{2}L^3\left(\frac{u_{A\infty}}{2}\right)^2\right]N_0' + \left\{\left[\frac{\rho}{2}L^3 U_r\right]N_r' v_r - \left[\frac{\rho}{2}L^3\right]N_\delta'(c - c_0)v_r\right\} + \left\{\left[\frac{\rho}{2}L^4 U_r\right](N_r' - m' x_G' u_r')r + \tfrac{1}{2}[\tfrac{\rho}{2}L^4]N_\delta'(c - c_0)r\right\} + \left[\frac{\rho}{2}L^3 c^2\right]N_\delta'\delta + \left[\frac{\rho}{2}L^5 U_r^{-1}\right]N_{rrv_r}' r^2 v_r + [\tfrac{\rho}{2}L^3 c^2]N_{eee}' e^3 \\ f_4 = \left(m' - Y_{\dot{v}_r}'\right)\left[\frac{\rho}{2}L^3\right](I_z' - N_{\dot{r}}')\left[\frac{\rho}{2}L^5\right] - \left(m' x_G' - N_{\dot{v}_r}'\right)\left[\frac{\rho}{2}L^4\right](m' x_G' - Y_{\dot{r}}')\left[\frac{\rho}{2}L^4\right] \end{cases} \tag{4}$$

in which ρ is the mass density of water; L is the length of the ship between perpendiculars; n are the propeller rps, C_R is the resistance coefficient of the vehicle; S is the wetted surface area of the ship; and c is the weighted average flow speed over rudder given by

$$c=\sqrt{\frac{A_P}{A_R}\left[(1-w)u_r+ku_{A\infty}\right]^2+\frac{A_R-A_P}{A_R}(1-w)^2u_r^2} \tag{5}$$

c_0 is the value of c when the propeller rotational speed and ship forward speed are in equilibrium in straight-ahead motion; A_P is the propeller area; A_R is the rudder area; w is the wake fraction; $u_{A\infty}$ is the induced axial velocity behind the propeller disk given by

$$u_{A\infty}=-(1-w)u+\sqrt{(1-w)^2u^2+\frac{8}{\pi}K_T(nD)^2} \tag{6}$$

K_T is the propulsive coefficient; D is the propeller diameter; and e is the effective rudder angle given by

$$e=\delta\frac{v}{c}+\frac{rL}{2c} \tag{7}$$

The simulation of the 20–20 zigzag manoeuvre was carried out in the Matlab platform using Eq. (3). The rudder angle and heading angle are recorded, as shown in Fig. 2.

Table 1
The main characteristics of "Esso Osaka" ship model (Moreira et al., 2007).

Parameter	Value	Unit
Length overall (L.O.A.)	3.430	m
Length between perpendiculars (L.P.P)	3.250	m
Breadth (B)	0.530	m
Draft (D)	0.217	m
Block coefficient	0.831	
Number of rudders	1	
Rudder area	0.0120	m^2
Propeller area	0.0065	m^2
Longitudinal CG	0.103	m
Displacement	319.40	kg

Table 2
The nondimensional hydrodynamic coefficients of "Esso Osaka" ship model (Moreira et al., 2007).

Coefficient	Value	Coefficient	Value
$(\mathbf{m}-\mathbf{Y}_{\dot{v}})'$	0.0352	N'_{vrr}	0.00611
$(\mathbf{I}_Z-\mathbf{N}_{\dot{r}})'$	0.00222	X'_{ee}	−0.00224
$\mathbf{Y}'_{\mathbf{v}}$	−0.0261	X'_{rvv}	−0.00715
$\mathbf{Y}'_{\mathbf{r}}$	0.00365	N'_{eee}	0.00116
$\mathbf{N}'_{\mathbf{v}}$	−0.0105	Y'_{vrr}	−0.0450
$\mathbf{Y}'_{\mathbf{r}}$	−0.00480	η'_1	-0.962×10^{-5}
$\mathbf{Y}'_{\delta}$	−0.00283	η'_2	-0.446×10^{-5}
$\mathbf{X}'_{\mathbf{vy}}+\mathbf{m}'$	0.0266	η'_3	0.0309×10^{-5}
$\mathbf{N}'_0$	−0.00028	m'	0.0181
		C'_R	0.00226

3. Control model and parameter identification

In order to design the steering autopilot, it is necessary to select a simple mathematical model with certain accuracy. Nomoto et al. (1957) proposed a linear model for the ship steering equations. The Nomoto's model is obtained by eliminating the sway velocity υ from (8) to obtain the Nomoto transfer function between r and δ_R.

$$\boldsymbol{M}\dot{v}+\boldsymbol{N}(u_0)v=\boldsymbol{b}\delta_R \tag{8}$$

where $v=[v,r]^T$ is the state vector,δ_R is the rudder angle;

$$\boldsymbol{M}=\begin{bmatrix}\mathrm{m}-Y_{\dot{v}}\mathrm{m}x_G-Y_{\dot{r}}\\ \mathrm{m}x_G-Y_{\dot{r}}I_z-N_{\dot{r}}\end{bmatrix}\boldsymbol{N}(u_0)=\begin{bmatrix}-Y_v\mathrm{m}u_0-Y_r\\ -N_v\mathrm{m}x_Gu_0-N_r\end{bmatrix}b=\begin{bmatrix}Y_\delta\\ N_\delta\end{bmatrix}$$

The Nomoto transfer function is:

$$\frac{r}{\delta}(s)=\frac{K(1+T_3s)}{(1+T_1s)(1+T_2s)} \tag{9}$$

where $T_i(i=1,2,3)$ are time constants and K is the gain constant. A 1st-order approximation is obtained by letting the effective time constant be equal to: $T=T_1+T_2-T_3$. Such that

$$\frac{r}{\delta}(s)=\frac{K}{(1+Ts)} \tag{10}$$

Since $r(s)=s\psi(s)$, finally:

$$\frac{\psi}{\delta}(s)=\frac{K}{s(1+Ts)} \tag{11}$$

$$\text{Time}-\text{domain}: T\ddot{\psi}+\dot{\psi}=K\delta \tag{12}$$

This model should only be used for low frequencies (Fossen, 2011). It is widely used for ship autopilot design due to its compromise between simplicity and accuracy.

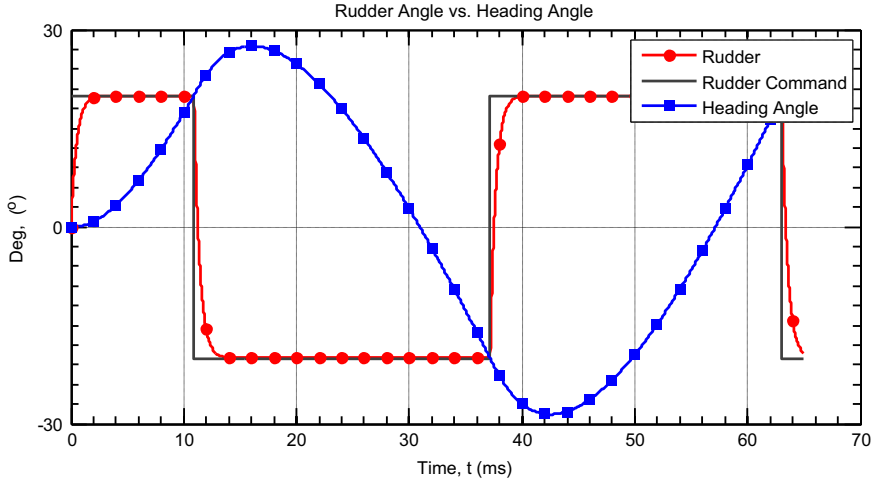

Fig. 2. The 20–20 zigzag manoeuvre simulation.

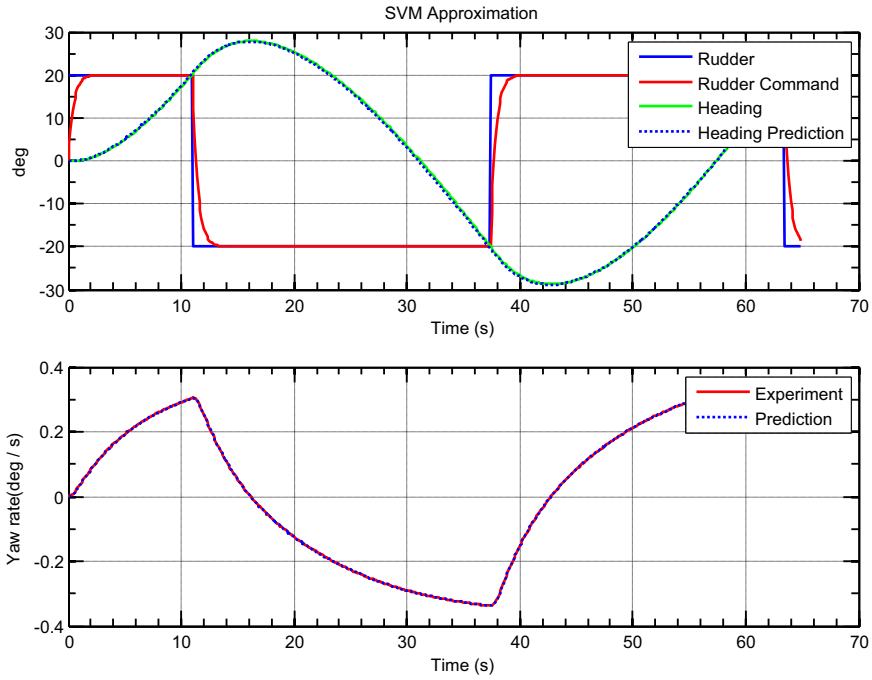

Fig. 3. Prediction of 20–20 Zigzag manoeuvre.

3.1. Parameter identification based on LS-SVM

System identification (Ljung, 1987) has been widely used in the modelling of ship motion. The Artificial Neural Networks (ANN) was used to create purely "input–output" models (Moreira and Guedes Soares, 2003, 2011, 2012), which is also called the black-box modelling. The advantage of ANN algorithm is that it does not imply any a priori structure of the ship mathematical model, but the disadvantage is that it cannot be extended, modified or tuned without full retraining which is not always possible (Sutulo and Guedes Soares, 2014). Recently a robust method, Support Vector Machine (Luo and Zou, 2009; Zhang and Zou, 2011; Luo et al., 2013', 2014) was applied to identify Abkowitz model for Mariner class surface ship and performed satisfactory.

The parameter identification method based on the Least Squares Support Vector Machine will be briefly introduced in this section. The parameter of the Nomoto model will be identified using LS-SVM. Support Vector Machine can minimise the estimation error, both the empirical risk and the structural risk. It can be designed to deal with sparse data. The input data are mapped into a high dimensional feature space using nonlinear mapping techniques, and the regression is carried out in feature space (Moreno-Salinas et al., 2013).

For regression purposes, SVM gives a general approximation function form:

$$y = \boldsymbol{w}^T \cdot \Phi(x) + b \tag{13}$$

where x is the input vector, $x \in \Re^n$, y is the output data, $y \in \Re$, b is the bias term, $\boldsymbol{w}$ is a weight matrix, $\Phi(\bullet)$ is a nonlinear function, which is mapping the input data to a high dimensional feature space. To satisfy the minimisation of structural risk, a cost-function is defined as following:

$$\begin{cases} \min\limits_{w,b,e} f(w,e) = \frac{1}{2}\boldsymbol{w}^T\boldsymbol{w} + \frac{1}{2}C\sum\limits_{i=1}^{l} e_i^2 \\ \text{subject to: } y_i = \boldsymbol{w}^T \cdot \Phi(x_i) + b + e_i \end{cases} \tag{14}$$

where $i = 1 \cdots l$, e_i is error variables, and C is the regularisation factor. The minimisation of $\boldsymbol{w}^T\boldsymbol{w}$ is closely related to the use of a weight decay term in the training of neural networks, and the $\sum\limits_{i=1}^{l} e_i^2$ controls the tradeoff between the empirical error and the model complexity.

The Lagrangian function is defined as:

$$\mathcal{L}(w,b,e,\alpha) = \frac{1}{2}\boldsymbol{w}^T\boldsymbol{w} + \frac{1}{2}C\sum_{i=1}^{l} e_i^2 - \sum_{i=1}^{l}\alpha_i\left[\boldsymbol{w}^T \cdot \Phi(x_i) + b + e_i - y_i\right] \tag{15}$$

where α_i are the Lagrange multipliers. The optimality conditions are defined by computing the derivatives of (15) with respect to w, b, e, α:

$$\begin{cases} \frac{\partial \mathcal{L}}{\partial w} = 0 \rightarrow w = \sum\limits_{i=1}^{l}\alpha_i\Phi(x_i) \\ \frac{\partial \mathcal{L}}{\partial b} = 0 \rightarrow \sum\limits_{i=1}^{l}\alpha_i = 0 \\ \frac{\partial \mathcal{L}}{\partial e_i} = 0 \rightarrow \alpha_i = Ce_i \\ \frac{\partial \mathcal{L}}{\partial \alpha_i} = 0 \rightarrow \boldsymbol{w}^T \cdot \Phi(x_i) + b + e_i - y_i = 0 \end{cases} \tag{16}$$

After elimination of variables w, and e_i from Eq. (16), and applying the kernel trick which allows working in high-dimensional feature spaces without explicit computations on them, the LS-SVM model for function estimation yields

$$y(x) = \sum_{i=1}^{l}\alpha_i K(x, x_i) + b \tag{17}$$

where $K(\bullet,\bullet)$ is the kernel function that represents an inner product between its operands. The kernel must be a positive definite kernel and must satisfy the Mercer condition (Mercer, 1909).

Usually, the Nomoto first-order model was given by

$$T\dot{r} + r = K\delta \tag{18}$$

So $x = [r_k, \delta_k]^T$ can be chosen as input data and $y = [r_{k+1}]$ as output data. From the previous discuss, the regularisation factor and the kernel function have an important effect on the convergence of LS-SVM. The linear kernel have to be chosen in order to obtain the parameters, The regularization factor C= 2544 is

chosen (Luo et al., 2013). The Nomoto time and gain constants (T, K) are the parameters to be identified. The K, and T were identified by using 20–20 Zigzag simulation data. The values obtained for K and T are: $K=0.1807\ s^{-1}$, $T=7.3970$ s. From Fig. 3, the identification and experimental heading curves are in good agreement.

3.2. PID heading controller with feedforward

Using the Nomoto constants obtained in the previous discussion, the PID heading controller is designed and the controller gains are calculated. Assuming that ψ is measured by a compass, consider the PID controller law:

$$\tau_N(s)=\tau_{PID}(s)=K_p(\psi_d-\psi)-K_d\dot{\psi}+K_i\int_0^t(\psi_d-\psi(\tau))d_\tau \tag{19}$$

where $K_p>0$, $K_d>0$ and $K_i>0$ are the regulator design parameters. Applying this control law to Nomoto 1st-order model (Eq. (12)), the closed-loop characteristic equation one can get:

$$T\sigma^3+(1+KK_d)\sigma^2+KK_p\sigma+KK_i=0 \tag{20}$$

By applying Routh's stability criterion, another simple intuitive way to do this is by noticing that δ can be written as (Fossen, 2011):

$$\tau_N(s)=\tau_{PID}(s)=K_p\left(1+T_ds+\frac{1}{T_is}\right)(\psi_d-\psi) \tag{21}$$

A continuous-time representation of the controller is

$$\tau_N(s)=\tau_{PID}(s)=K_p(\psi_d-\psi)+K_d(\dot{\psi}_d-\dot{\psi})+K_i\int_0^t(\psi_d-\psi(\tau))d_\tau \tag{22}$$

where τ_N is the controller yaw moment, $K_d=K_pT_d$, and $K_i=K_p/T_i$. The controller gains can be found by pole placement in terms of the design parameters ω_n and ζ, though:

$$K_p=\frac{\omega_n^2T}{K}>0$$

$$K_d=\frac{2\zeta\omega_nT-1}{K}>0$$

$$K_i=\frac{\omega_n^3T}{10K}>0$$

where ω_n is the natural frequency and ζ is the relative damping ratio of the first order system. In this case, $\omega_n=1$ rad/s and critical damping $\zeta=1$. Thus, the following controller gains are obtained: $K_p=40.9353$, $K_d=76.3365$ and $K_i=0.0587$.

In order to achieve accurate and rapid course-changing manoeuvres, a feedforward term can be applied to the controller. The PID-controller for full state feedback is given by:

$$\tau_N(s)=\tau_{FF}(s)+K_p(1+T_ds+\frac{1}{T_is})(\psi_d-\psi) \tag{23}$$

where τ_{FF} is a feedforward term to be decided. Using Nomoto's first-order model as basis for feedforward, suggests that reference feedforward should be included according to

$$\tau_{FF}=\frac{T}{K}r^d+\frac{1}{K}r_d \tag{24}$$

4. Vector field path following

In order to follow the predefined path accurately, the ASVs have to minimise the heading error and the cross-track error. The vector field method calculates a vector field around the path to be tracked. The vectors in the field are directed towards the path to be followed and in the desired direction of travel. The main idea of this approach is that vector field indicate the direction of flow. If the vehicle follows the VF direction then it will follow the path. Fig. 4 shows the examples of vector fields for straight path. This approach is now widely used in the guidance of UAVs (Nelson et al., 2007, Zhou and Schwager, 2014, Lim et al., 2014). In (Sujit et al., 2014), a detailed analysis of path-following algorithms for UAVs was performed. The results show that vector field path-following technique more accurately follows the path than the other techniques and also requires the least control effort.

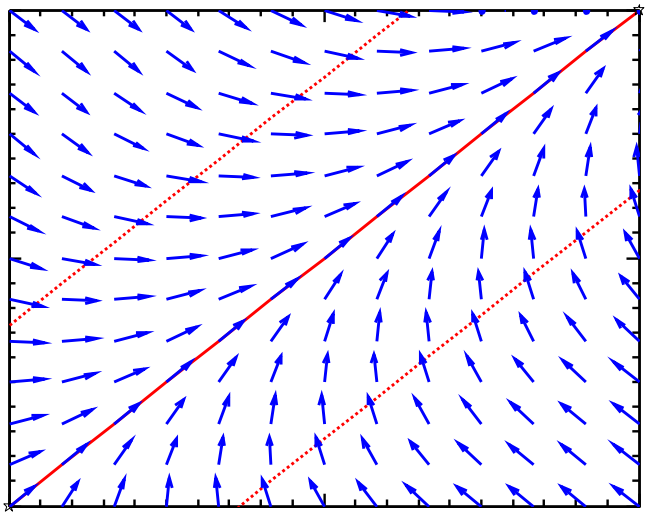

Fig. 4. Examples of the vector field. (For interpretation of the references to colour in this figure legend, the reader is referred to the web version of this article.)

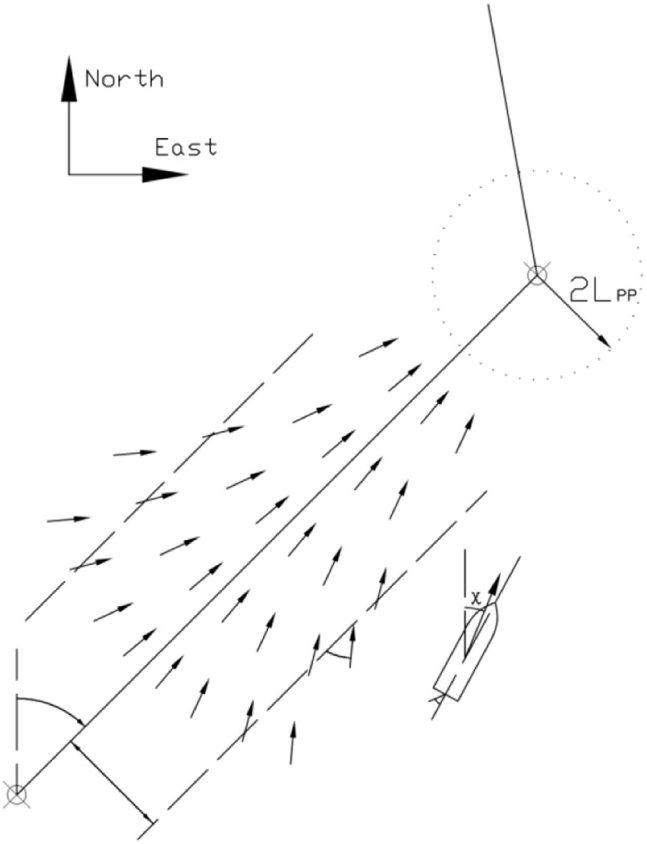

Fig. 5. Vector field guidance geometry.

Table 3
Variables of vector field for straight path following.

Variables	Description
χ^f	Heading between the waypoints
χ^e	Entry heading angle ($0<\chi^e\leq\frac{\pi}{2}$)
χ^c	Commanded heading
τ	Transition region boundary distance
y_e	Cross-track error
w_{xj}, w_{yj}	waypoints
(x, y)	Current location of the ASV
d	Distance from the waypoint $j+1$
k	Transition gain, $k>1$
ρ	The side of the path that the ASV is on, having a value of ± 1

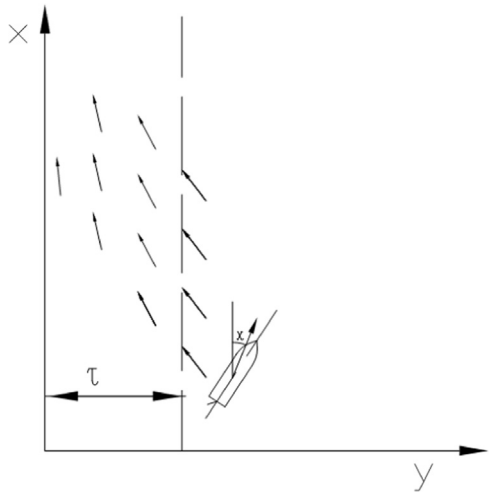

Fig. 6. Vector field guidance geometry for $y>0$ and $\chi^f=0$.

From the previous discussion, (1), (2) and (3) can be expressed as

$$\dot{x}=U_r\cos\chi \tag{25}$$

$$\dot{y}=U_r\sin\chi \tag{26}$$

where $\chi=\psi+\beta$, is the course angle, ψ is the heading angle, β is the sideslip angle. From Section 3, we designed a PID heading controller and that the resulting dynamics are represented by the first order system

$$\dot{\chi}=\alpha(\chi^c-\chi) \tag{28}$$

where χ^c is the commanded track heading, and α is a known positive constant, which characterizes the speed of response of course-hold autopilot loop.

4.1. Vector field algorithm

As shown in the Figs. 4 and 5, the solid line segment is the straight path to be followed, the red dashed lines, which lie at a distance τ on each side of the path, indicated the transition region. In order to follow this path, a vector field of desired track headings is constructed. When the ASV is far away from the path, such as $d>\tau$, the algorithm will guide the vehicle to travel towards the path at a constant desired heading or entry angle χ^e. When the vehicle is inside the transition region ($d<\tau$), the desired heading begins to transition from χ^e to the heading along the desired path χ^f, the rate of transition is controlled by a gain, $k>1$. Table 3 shows a list of variables used for the straight path following algorithm. In order to achieve the desired performance, the parameter τ, χ^e and k can be chosen based on the capabilities of the ASV.

The basic idea of the algorithm is to find where the ASV is in the vector field and then command a heading that will result in the ASV matching the desired heading as defined by the algorithm. The vector field algorithm in pseudocode is shown in the following:

Algorithm. : Vector field algorithm

BEGIN:

1. $\chi^f:=\text{atan2}(w_{yj+1}-w_{yj}, w_{xj+1}-w_{xj})$; // calculate heading from waypoint $j+1$ to j;
2. $y_e:=\frac{[(w_{xj+1}-w_{xj})(y-w_{yj})-(w_{yj+1}-w_{yj})(x-w_{xj})]}{\sqrt{(w_{yj+1}-w_{yj})^2+(w_{xj+1}-w_{xj})^2}}$; //calculate the distance from the path;
3. $\rho:=\text{sign}(y_e)$; // decide which side of the path ASV is on;
4. $d:=\sqrt{(w_{yj+1}-y)^2+(w_{xj+1}-x)^2}$; // calculate distance from the waypoint $j+1$;
5. **If** $d>2L_{PP}$ **Then**
6. $j:=j+1$; // ASV switch to next waypoint;
7. **Else**
8. **If** $|y_e|>\tau$ **Then** // distance from the path is greater than τ;
9. $\chi^d:=\chi^f-\rho\chi^e$; // set vector field heading;
10. $\chi^c:=\chi^d$; // set command heading to the ASV;
11. **Else**
12. $\chi^d:=\chi^f-\rho(|y_e|_{\tau})^k\chi^e$; // set vector field heading;
13. $\chi^c:=\chi^d-(\frac{k\chi^e U_r}{\alpha\tau^k})(|y_e|)^{k-1}\sin\chi$; // set command heading to the ASV;
14. **End If**
15. **End If**

End

4.2. Vector field stability analysis

In this section, Lyapunov function will be used to prove the stability of the vector field algorithm used for guidance. According the previous discussion, it is necessary to prove that the ASV will enter the transition region ($d<\tau$) in finite time when the distance is greater than Transition region boundary distance. Then the proof will be made that the cross-track error and heading track error will approach zero asymptotically (Nelson et al., 2006). When $|y_e|>\tau$, without loss of generality, consider the case shown in Fig. 6, where the path to be followed is the x-axis with $\chi^f=0$ implying that $y_e=y$. So we get

$$\chi^c=\chi^d=-\rho\chi^e \tag{29}$$

Lyapunov function can be defined:

$$V(\chi)=\frac{1}{2}\tilde{\chi}^2 \tag{30}$$

where $\tilde{\chi}=\chi^d-\chi$, then taking the derivative along the solution of the system gives

$$\dot{V}(\chi)=\tilde{\chi}\dot{\tilde{\chi}}=\tilde{\chi}\left(\dot{\chi}^d-\dot{\chi}\right) \tag{31}$$

where χ^d is the desired heading angle and is constant, considering Eq. (28), so

$$\dot{V}(\chi)=-\tilde{\chi}\dot{\chi}=-\tilde{\chi}\alpha(\chi^c-\chi)=-\alpha\tilde{\chi}\left(\chi^d-\chi\right)=-\alpha\tilde{\chi}^2 \tag{32}$$

From Eq. (32), the conclusion can be get that $\dot{V}$ is negative semidefinite and the guidance system is stable. Because $\dot{\tilde{\chi}}=-\alpha\tilde{\chi}$

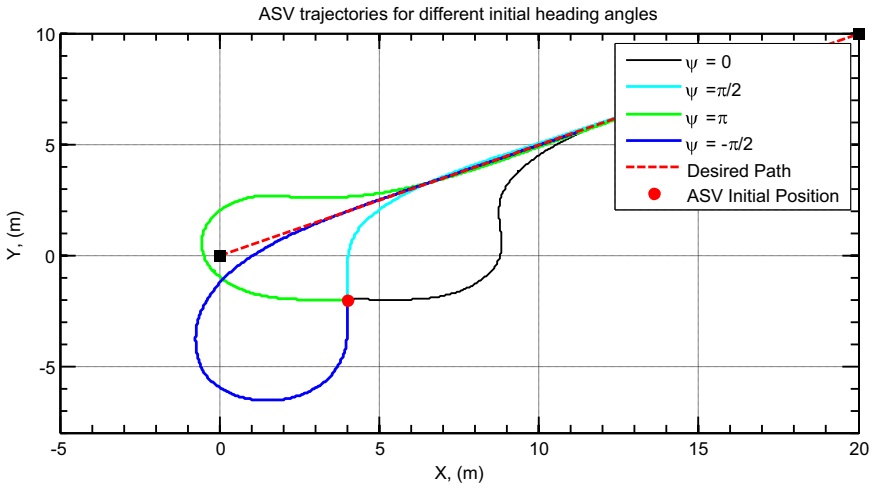

Fig. 7. ASV trajectories for the different initial heading angles with $k=1$ and $\tau=2*L_{PP}$.

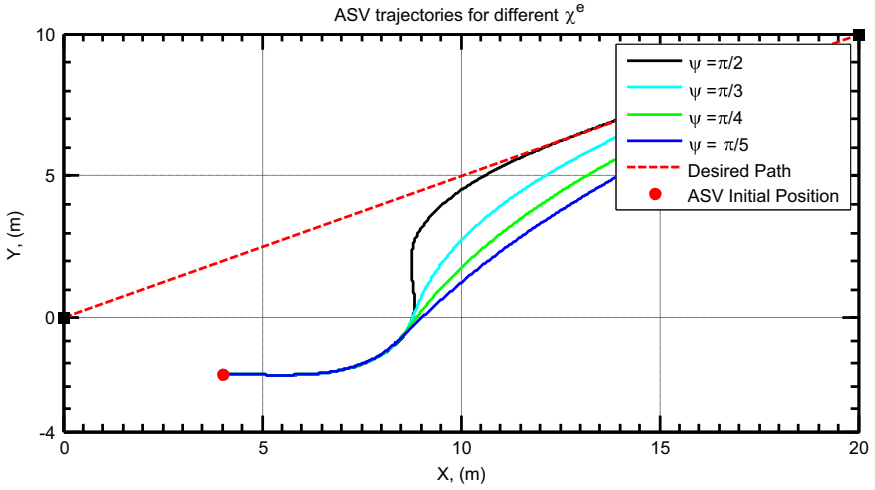

Fig. 8. ASV trajectories for the different χ^e with $k=1$ and $\tau=2*L_{PP}$.

which implies that $\tilde{\chi}(t)=e^{-\alpha t}\tilde{\chi}(t_0)$, so the heading track will therefore converge exponentially to $-\rho\chi^e$.

When $y_e(t_0)>\tau$ and $0<\chi(t_0)<\pi$, the cross-track error $y_e(t)$ will increase initially, However, as $\chi(t)$ decreases exponentially it approaches $-\rho\chi^e$, there must exit an $\epsilon'>0$ such that χsuc will eventually enter the set $M\triangleq[-\pi+\epsilon',-\epsilon']$. When $\chi(t)\in M$, there exists $\epsilon''>0$ such that $y^e=y^{U_r\sin\chi\le-\epsilon''}$ which implies that the decrease in y_e is bound by a constant rate which implies that $y_e(t)$ will enter the transition region in finite time.

When the vehicles are inside the transition region, without loss of generality, the case that the ASV follows the x-axis and the conditions where $y(t_0)$ is positive is considered, from the previous discussion, the desired heading angle can be got by:

$$\chi^d=-(\chi^e)(\frac{y_e}{\tau})^k \tag{33}$$

Lyapunov function can be defined:

$$V(y_e,\chi)=\frac{1}{2}y_e^2+\frac{1}{2}\tilde{\chi}^2 \tag{34}$$

where $\tilde{\chi}=\chi^d-\chi$, and taking the derivative along the solution of the system gives

$$\dot{V}(y_e,\chi)=y_e\dot{y}_e+\tilde{\chi}\dot{\tilde{\chi}}=y_e\dot{y}+\tilde{\chi}\left(\dot{\chi}^d-\dot{\chi}\right)==y_eU_r\sin(\chi^d-\tilde{\chi})+\tilde{\chi}\left(\dot{\chi}^d-\dot{\chi}\right)$$
$$=y_eU_r\sin(-(\chi^e)\left(\frac{y_e}{\tau}\right)^k-\tilde{\chi})+\tilde{\chi}\left(\left(\frac{-k\chi^eU_r}{\tau^k}\right)y_e^{k-1}\sin\chi-\alpha(\chi^c-\chi)\right) \tag{35}$$

Choosing χ^c as in (34) gives

$$\dot{V}(y_e,\chi)=y_eU_r\sin(-(\chi^e)(\frac{y_e}{\tau})^k-\tilde{\chi})-\alpha\tilde{\chi}^2 \tag{36}$$

When $-\pi<-(\chi^e)\left(\frac{y_e}{\tau}\right)^k-\tilde{\chi}<0$, the derivative of Lyapunov function $V^e,\chi)$ will be negative.

From Eq. (33), when $-\pi\le\chi\le0$, the $V(y_e,\chi)$ will be negative semi-definite. Define the set $M\triangleq\{(y_e,\chi):-\pi\le\chi\le0,-\tau\le y_e\le\tau\}$, and note that M is compact and that the boundary of M is a non-invariant level curve of $V(y_e,\chi)$. Therefore standard Lyapunov arguments imply that M is a positively invariant set. The proof is therefore complete if it is possible to show that the system trajectory enters M in finite time.

Differentiating the equation $\tilde{\chi}=\chi^d-\chi$ and using equation $\chi^c=\chi^d-(\frac{k\chi^eU_r}{\alpha\tau^k})y_e^{k-1}\sin\chi$, leads to $\dot{\tilde{\chi}}=-\alpha\tilde{\chi}$, which implies that $\tilde{\chi}(t)=e^{-\alpha t}\tilde{\chi}(t_0)$. Solving for $\chi(t)$ results in

$$\chi(t)=(1-e^{-\alpha t})\left[-\chi^e\left(\frac{y_e}{\tau}\right)^k\right]+e^{-\alpha t}\tilde{\chi}(t_0) \tag{37}$$

From Eq. (37), if the cross-track error $y_e(t)$ remains in the transition region, the trajectory of the system will enter M in finite time. However, the initial orientation of the ASV may force the system to leave the transition region ($|y_e|>\tau$). If this happens,

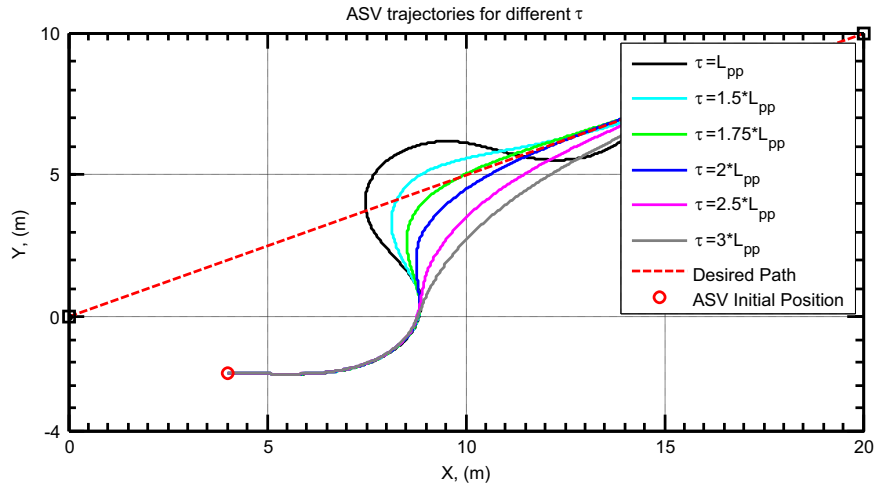

Fig. 9. ASV trajectories for the different τ with $k=1$ and $\chi^e=\frac{\pi}{2}$.

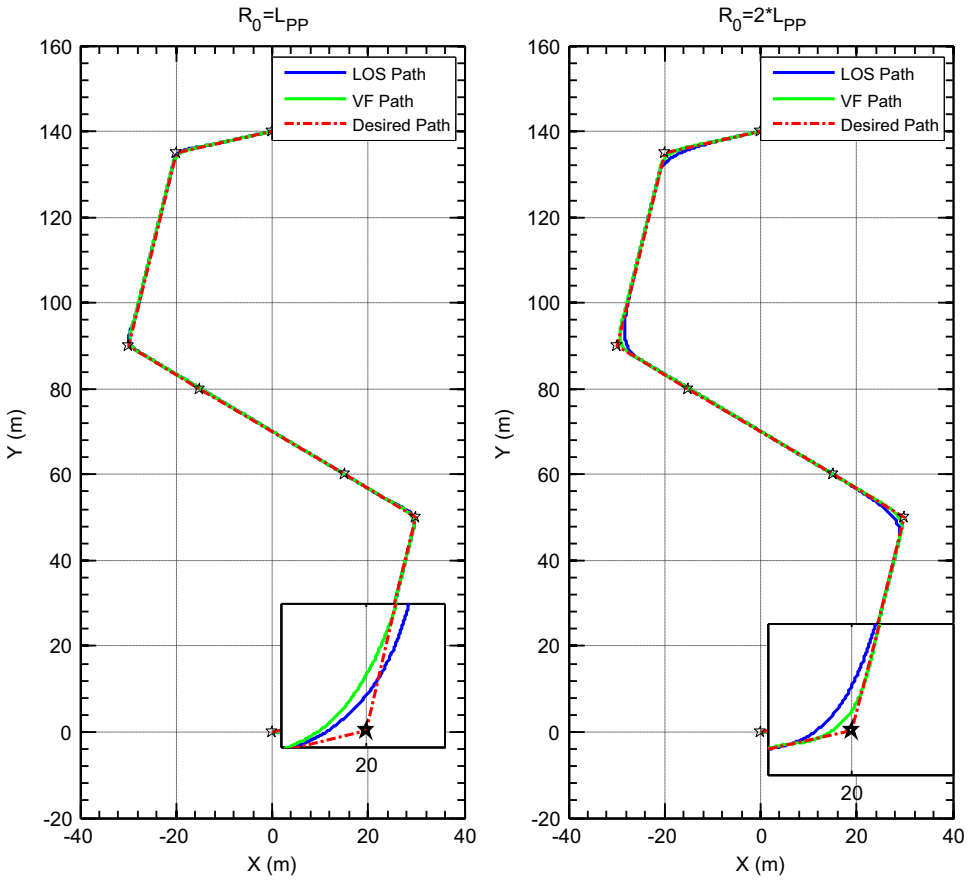

Fig. 10. x–y plot of the simulated and desired geometrical path for $R_0=L_{PP}$ and $R_0=2L_{PP}$ based on LOS and VF.

according the previous discussion, it is possible to see that the system will re-enter the transition region in finite time and that the heading upon re-entry will be in the set $(-\pi,0)$ which implies that upon re-entry, the system trajectory will be in M.

5. Case study: simulation results

In this section simulation studies will be presented to study the performance of the VF with different values of the parameter χ^e, τ, k and the initial heading angles. Another simulation will be carried out to compare the trajectories based on LOS algorithm using a constant circle (2^*L_{PP}) and the vector field. Fig. 7 shows the ability of VF to track the straight line with the different initial heading angle ($\psi_0=0,\frac{\pi}{2},\pi,-\frac{\pi}{2}$). From this figure it is possible to see that the vector field can always guide the ASV to follow the predefined the path whenever the initial heading varies.

Further, in order to study the sensitivity of the model to χ^e and τ, two more simulation tests are performed. In the first test, the parameter χ^e is varied between 0 and $\frac{\pi}{2}$ while the parameters

$\tau = 2 * L_{PP}$, $k = 1$ and the initial heading angle is zero. The results are shown in Fig. 8. The angle χ^e determined the angle of approach to the path, high χ^e will force the ASV to move towards the path quickly, resulting in quick convergence. Lower χ^e values increase the convergence time and the cross-track error.

In the second simulation test, the parameter τ is varied while holding $\chi^e = \frac{\pi}{2}$, $k = 1$ the initial heading angle is zero. The parameter τ is the width of the transition region near the predefined path, as shown in Fig. 9. The parameter τ determined the convergence time. The time taken to converge onto the path is high when τ is small, such as $\tau = L_{PP}$. However, with an increase in τ, the ASV converges quickly onto the path. With further increase in τ, the time taken to converge onto the path increase. From Fig. 9, we can see that $\tau = 2 * L_{PP}$ is a better choice for the width of the transition region.

In order to compare the performance of autonomous surface vehicles using LOS and vector field, another simulation studies will be presented here. The parameter $\chi^e$is $\frac{\pi}{2}$, τ is $2L_{PP}, k$ is 1 and the initial heading angles is zero. One trajectory was defined consisting of 9 waypoints and desired speed. The desired speed is kept constant with a value of 0.21 m/s, which corresponds to a Froude number $F_n = 0.0372$. Firstly the two methodologies are compared for two different radius of acceptance: $R_0 = L_{PP}$ and $R_0 = 2L_{PP}$. The trajectory is given by

The first trajectory:		
Wp1=(0,0)m,	Wp2=(20,5)m,	Wp3=(30,50)m,
Wp4=(15,60)m,	Wp5=(−15,80) m,	Wp6=(−30,90) m,
Wp7=(−20,135)m,	Wp8=(0,140)m,	Wp9=(20,145)m,
The desired speed:		
$r^b = 0.21$ m/s		
$(F_n = 0.0372)$		

From Fig. 10, one can see that the vector field guidance method has a better performance than the LOS and one can also conclude that the radius of acceptance is better chosen as $2L_{PP}$, which will result small cross-track errors.

Another trajectory is defined as follow:

The second trajectory:	
Wp1=(0,0)m,	Wp2=(20,10)m,

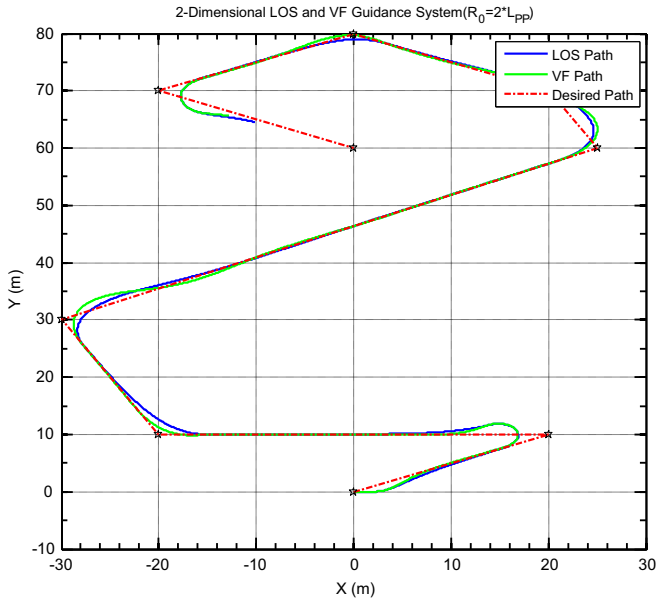

Fig. 11. *xy*-plot of the simulated and desired geometrical path of the second trajectory using LOS and VF methods.

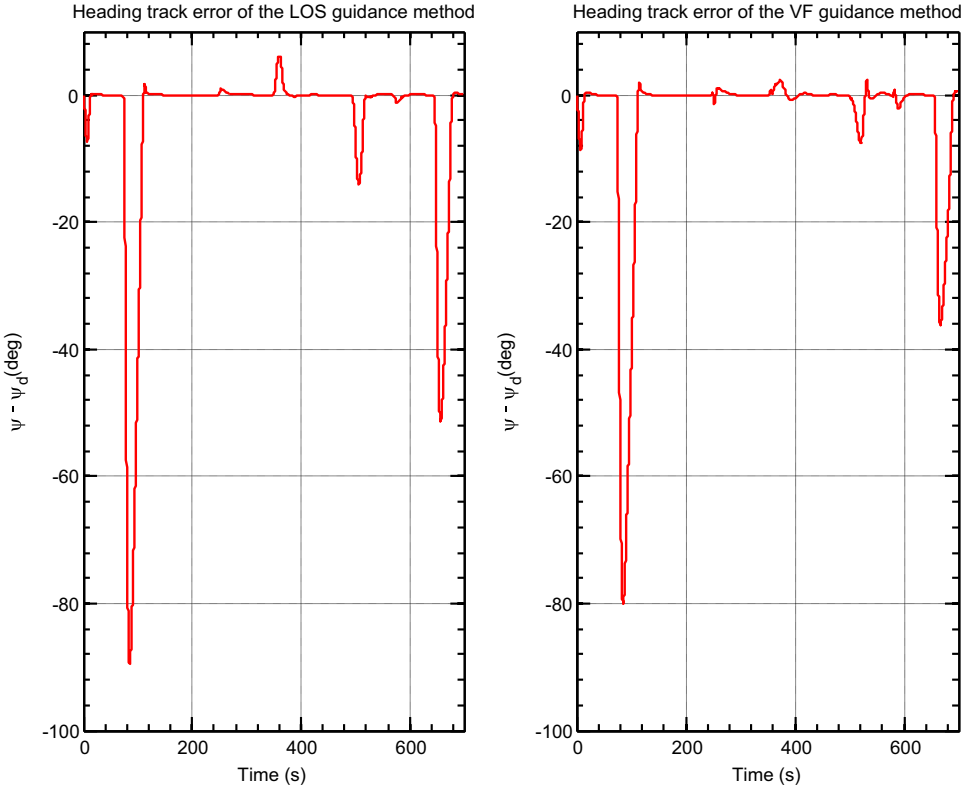

Fig. 12. The error $\psi - \psi_d$ for the second simulated trajectory.

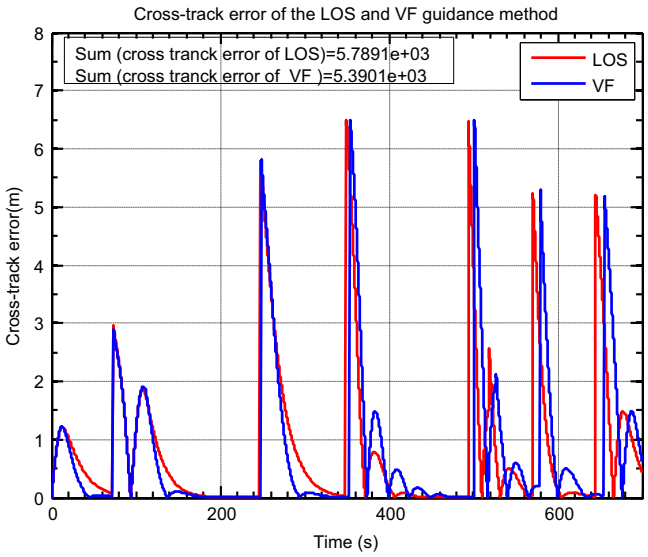

Fig. 13. The plot of the cross-track error for the second simulated trajectory.

		Wp3=(−20,10) m,
Wp4=(−30,30)m, Wp7=(0,80)m,	Wp5=(25,60)m, Wp8=(−20,70) m,	Wp6=(20,70)m, Wp9=(0,60)m,
The desired speed:		
$r^b = 0.21$ m/s (F_n=0.0372)	If $t_1 \le t \le t_3$	
$r^b = 0.43$ m/s (F_n=0.0762)	If $t_3 < t \le t_6$	
$r^b = 0.27$ m/s (F_n=0.0487)	If $t_6 < t \le t_9$	

In this simulation the radius of acceptance for all way points was set to two ship lengths ($2L_{PP}$). Fig. 11 shows a *xy*-plot of the second trajectory simulation of the ASV position together with the predefined path consisting of straight line segments for the LOS and VF methods. From the Fig, it is possible to conclude that the vector field has a small cross-track error and a better performance. Figs. 12 and 13 present the heading tack error and cross-track error obtained through the difference between the actual values and the desired values for LOS and vector field methods, respectively.

In Figs. 10–13, it is seen that the convergence to the desired trajectory is done successfully and is improved with the vector field. So it can be concluded that the new methodology presented here can be applied with success to minimise the heading track error and cross-track error between the actual and the desired path of the vehicle as can be seen from Figs. 12 and 13.

6. Conclusion

In this paper a new method for autonomous surface vehicle path following has been introduced. The vector field is used for guidance system of autonomous surface vehicle. The vector filed method calculates vectors in the field, which are directed towards the path to be followed. The stability analysis is carried out by using Lyapunov function. It has been shown that controlling heading rate yields asymptotic following for the predefined path. Moreover, a PID heading controller and speed controller were developed. The Nomoto model is chosen as the control model and the parameters are obtained by using the least-square support vector machine. Simulation test based on the mathematical model of the ASV are carried out to determine the parameter of the vector field algorithm. The performance of the guidance and control system based on LOS and vector field is compared. The results demonstrate that the vector field have a better performance. The presented approach is a practical and robust method for accurate path following, and can be extended to higher dimensional control and guidance problems.

Acknowledgements

This work was performed within the Strategic Research Plan of the Centre for Marine Technology and Ocean Engineering, which is financed by Portuguese Foundation for Science and Technology (Fundação para a Ciência e Tecnologia – FCT).

References

Abkowitz, M.A., 1980. Measurement of hydrodynamic characteristics from ship maneuvering trials by system identification. SNAME Trans. 88, 283–318.
Breivik, M., Fossen, T.I., 2009. Guidance Laws for autonomous underwater vehicles. In: Inzartsev, A.V. (Ed.), Underwater Vehicles. INTECH Education Publishing, Vellore, India, pp. 51–76 (chapter 4).
Børhaug, E., Pettersen, K., 2005. Cross-track control for underactuated autonomous vehicles. In: Proceedings of Decision and Control, European Control Conference. Seville, Spain, pp. 602–608.
Chen, C., Shiotani, S., Sasa, K., 2013. Numerical ship navigation based on weather and ocean simulation. Ocean Eng. 69 (1), 44–53.
Fossen, T.I., 2002. Marine Control Systems: Guidance, Navigation and Control of Ships, Rigs and Underwater Vehicles. Marine Cybernetics, Trondheim, Norway.
Fossen, T.I., 2011. Handbook of Marine Craft Hydrodynamics and Motion Control. Wiley Published, Trondheim, Norway.
Fredriksen, E., Pettersen, K.Y., 2006. Global κ-exponential way-point maneuvering of ships: theory and experiments. Automatica 42 (4), 677–687.
Fossen, T.I., Pettersen, K.Y., 2014. On semiglobal exponential stability (USGES) of proportional line-of-sight guidance laws. Automatica 50 (11), 2912–2917.
Frew, E.W., Lawrence, D.A., Morris, S., 2008. Coordinated standoff tracking of moving targets using Lyapunov guidance vector fields. J. Guid. Control Dyn. 31, 17.
Gonçalves, V.M., Pimenta, L.C.A., Maia, C.A., Dutra, B.C.O., Pereira, 2010. Vector fields for robot navigation along time-varying curves in dimensions. IEEE Trans. Robot. 26 (4), 647–659.
Loe, Ø.A.G., 2008. Collision Avoidance for Unmanned Surface Vehicles (Master thesis). Norwegian University of Science and Technology, Trondheim, Norway.
Lekkas, A.M., Fossen, T.I., 2013. Line-of-sight guidance for path following of marine vehicles. In: Gal, O. (Ed.), Advanced in Marine Robotics. LAP LAMBERT Academic Publishing, pp. 63–92 (chapter 5).
Lekkas, A.M., Fossen, T.I., 2014. Integral LOS path following for curved paths based on a monotone cubic hermite spline parametrization. IEEE Trans. Control Syst. Technol. 22 (6), 2287–2301.
Lim, S.L., Jung, W., Bang, H,. 2014. Vector field guidance for path following and arrival angle control. In: Proceedings of the 2014 International Conference on Unmanned Aircraft Systems. Orlando, USA. pp. 329–338.
Ljung, L., 1987. System Identification: Theory for the User. Prentice-Hall, Englewood Cliffs, NJ.
Luo, W.L., Guedes Soares, C., Zou, Z.J., 2013. Parameter identification of ship manoeuvring model based on particle swarm optimization and support vector machines. In: Proceedings of the 32nd International Conference on Ocean, Offshore and Arctic Engineering Nantes, France.
Luo, W.L., Moreira, L., Guedes Soares, C., 2014. Manoeuvring simulation of catamaran by using implicit models based on support vector machines. Ocean Eng. 82, 150–159.
Luo, W.L., Zou, Z.J., 2009. Parametric identification of ship manoeuvring models by using support vector machines. J. Ship Res. 53 (1), 19–30.
Mercer, J., 1909. Functions of positive and negative type and their connection with the theory of integral equations. Philos. Trans. R. Soc. A Math. Phys. Eng. Sci. 209, 415–446.
Moreira, L., Guedes Soares, C., 2003. Dynamic model of maneuverability using recursive neural networks. Ocean Eng. 30 (13), 1669–1679.
Moreira, L., Guedes Soares, C., 2011. Autonomous ship model to perform manoeuvring tests. J. Marit. Res. 8 (2), 29–46.
Moreira, L., Guedes Soares, C., 2012. Recursive neural network model of catamaran manoeuvring. Int. J. Marit. Eng. 154, A-121–A-130.
Moreira, L., Fossen, T.I., Guedes Soares, C., 2007. Path following control system for a tanker ship model. Ocean Eng. 34, 2074–2085.
Moreno-Salinas, D., Chaos, D., Cruz, J.M., Aranda, J., 2013. Identification of a surface marine vessel using LS-SVM. J. Appl. Math. 2013, 1–11.

Nelson, D.R., Barber, D.B., Mclain, T.W., Beard, R.W., 2006. Vector field path following for small unmanned air vehicles. In: Proceedings of the 2006 American Control Conference. Minneapolis, Minnesota, USA, pp. 5788–5794.

Nelson, D.R., Barber, D.B., Mclain, T.W., 2007. Vector field path following for miniature air vehicles. IEEE Trans. Robot. 23 (3), 519–529.

Nomoto, K., Taguchi, T., Honda, K., Hirano, S., 1957. On the Steering Qualities of Ships. International Shipbuilding Progress, p. 4.

Perera, L.P., Moreira, L., Santos, F.P., Ferrari, V., Sutulo, S., Guedes Soares, C., 2012. A navigation and control platform for real-time manoeuvring of autonomous ship models. In: Proceedings of the 9th IFAC Conference on Manoeuvring and Control of Marine Craft (MCMC2012). Arenzano, Italy.

Sujit, P.B., Saripalli, S., Borges Sousa, J., 2014. Unmanned aerial vehicle path following: a survey and analysis of algorithms for fixed-wing unmanned aerial vehicless. Control Syst. IEEE 34 (1), 42–59.

Sutulo, S., Guedes Soares, C., 2014. An algorithm for offline identification of ship manoeuvring mathematical models from free-running tests. Ocean Eng. 79, 10–25.

Sutulo, S., Moreira, L., Guedes Soares, C., 2002. Mathematical models for ship path prediction in manoeuvring simulation systems. Ocean Eng. 29, 1–19.

Vettor, R., Guedes Soares, C., 2015. Multi-objective evolutionary algorithm in ship route optimization. In: Guedes Soares, C., Santos, T.A. (Eds.), Maritime Technology and Engineering. Taylor & Francis Group, London, UK, pp. 865–876.

Zhang, X.G., Zou, Z.J., 2011. Identification of Abkowitz model for ship manoeuvring motion using ε-support vector regression. J. Hydrodyn. 23 (3), 353–360.

Zhou, D., Schwager, M., 2014. Vector field following for quadrotors using differential flatness. In: Proceedings of the 2014 IEEE International Conference on Robotics & Automation (ICRA). Hong Kong, China, pp. 6567–6572.